ACS APPLIED BIO MATERIALS

www.acsabm.org Article

Seaweed Superheroes: *Cystoseira barbata*-Incorporated Electrospun Fibers for Lead Ion Sequestration

Fatma Rabia Karaduman, Saniye Türk Çulha, and Nesrin Horzum*

Cite This: *ACS Appl. Bio Mater.* 2024, 7, 5345−5358 Read Online

ACCESS | Metrics & More | Article Recommendations | Supporting Information

ABSTRACT: The efficient removal of lead ions at low concentrations is paramount in combating the significant threat posed by water pollution resulting from industrial activities and population growth. In this study, electrospun *C. barbata*/PAN fibers were developed to efficiently remove lead(II) ions from water. The morphology, structure, and mechanical properties of the fibers were examined, highlighting that the augmentation of the surface area through the conversion of *C. barbata* into the polymer fibers facilitates increased metal bonding sites during sorption. *C. barbata*/PAN fibers exhibited superior characteristics, including higher surface area, smaller pore size, and increased pore volume, compared to powdered *C. barbata*. The effects of factors such as shaking time, algae percentage, sorbent amount, pH, metal concentration, and temperature on Pb(II) sorption were investigated by the batch method. At an initial ion concentration of 100 μg L^{-1} and pH 4.0, *C. barbata* (5 wt %)/PAN fiber demonstrated a notable sorption efficiency of 89−90% (270 μg/g) after 60 min. The equilibrium data align with the Freundlich and Dubinin−Radushkevich isotherm models, whereas the pseudo-second-order kinetic model provides the most suitable description. The characterization of fibers after sorption revealed that carboxyl, hydroxyl, and sulfonyl groups play an active role in Pb(II) sorption.

KEYWORDS: *Algae, Electrospinning, Heavy metal, Nanofiber, Biosorption*

INTRODUCTION

Water pollution is a significant environmental issue, and finding efficient ways to remove contaminants has been of significant research interest. The main categories of pollutants found in water include physical (suspended sediment or organic material), chemical (inorganic such as industrial chemicals, heavy metals, nutrients, and organic like detergents, industrial dyes, oil spills, pesticides, petroleum hydrocarbons, pharmaceuticals), biological, such as pathogens (bacteria, viruses, parasites, etc.), and thermal or radioactive substances.[1] Among them, heavy metals have become one of the important water pollutants due to the increasing population, rapid industrialization, and growing industrial and human activities, such as the textile industry, metal smelting, batteries, pesticides, the mining industry, petrochemicals, paper production, and electrolysis applications.[2] Furthermore, because of their toxicity, protracted presence in water, accumulation in living things and the food chain, and lack of biodegradability, heavy metal ions pose a serious threat.[3] When exposed to these metals, they can cause severe critical health issues for humans such as organ toxicity, decreased development and growth, cancer, and also death.[4] Therefore, the removal of heavy metals is very important for protecting human health and the environment. The presence of lead (Pb) and its compounds in heavy metals is a serious environmental and health problem. The World Health Organization has set the maximum acceptable Pb limits as 10 μg L^{-1}, and the action level for the Environmental Protection Agency is 15 μg L^{-1} in drinking water.[5]

A variety of methods, including physical (sorption, coagulation, flocculation, ion exchange, membrane separation) and chemical (chemical precipitation, electrochemical treatment, electrodialysis, reverse osmosis, solvent extraction), have been used for the removal of heavy metals from aqueous systems.[5] The widely used water treatment method is sorption due to its low cost, high efficiency, easy operation, renewable, environmentally friendly, and versatile properties. Many different sorbents, such as activated carbon, oxide minerals, polymer resins, and biological materials, have been used to adsorb heavy metal ions effectively.[2] Recently, in the pursuit of environmental sustainability and protection, researchers

Received: April 23, 2024
Revised: July 4, 2024
Accepted: July 5, 2024
Published: July 11, 2024

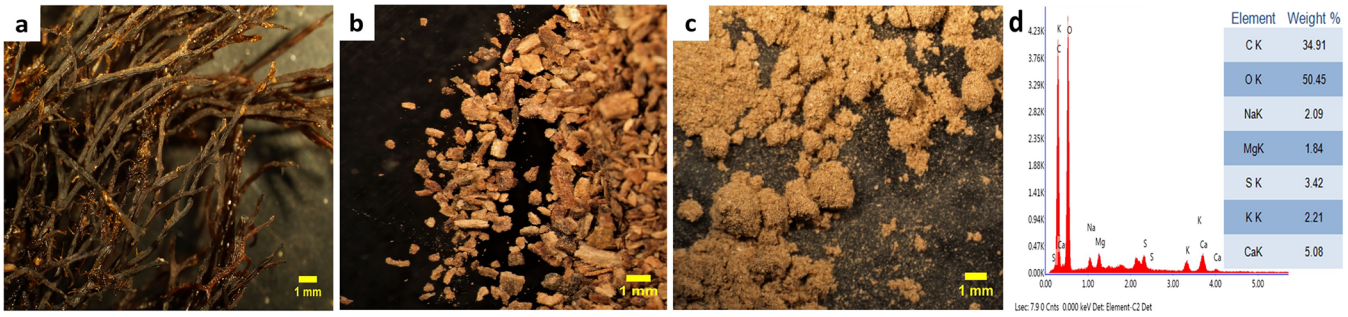

Figure 1. Stereo microscope images of *C. barbata*: (a) raw, (b) milled, (c) sieved, and (d) EDX spectrum of the *C. barbata* powder.

evaluated several biosorbents such as algae, fungi, bacteria, and yeast for the remediation of polluted water in the biosorption concept.[6] Algae are biosorbents with an excellent metal binding capacity. Because their cell walls are composed of cellulose, carotenoids, lipids, polysaccharides, protein, and vitamins. Characteristic functional groups such as amino, carboxyl, hydroxyl, phosphate, sulfhydryl, and sulfate contribute to metal biosorption with different mechanisms, mainly ion exchange, complexation, and coordination.[6,7] Brown algae are the most preferred biosorbent because they offer better biosorption uptake than red or green algae.[8] In particular, alginic acid, alginates (the sodium/calcium salt of alginic acid), and fucoidan (sulfated polysaccharides) present in the cell walls of brown algae offer carboxyl groups, making them potentially excellent materials for heavy metal binding.[6] The frequently used brown algae sorbents are *Sargassum filipendula, S. muticum, S. fluitans, S. glaucescens, S. wightii, Laminaria digitata, L. japonica, Fucus vesiculosus, F. spiralis, Macrocystis pyrifera, M. integrifolia, Padina pavonica, Undaria pinnatifida,* and *C. barbata*.[8,9] Among them, *C. barbata* is widespread in the Mediterranean and Eastern Atlantic Ocean coasts and the Black Sea.[10] The cell wall of *C. barbata* is poor in cellulose but rich in alginic acid and total phenol content. It contains various carotenoids such as chlorophyll a, b, and fucoxanthin as pigment material and laminarin, sulfated polysaccharides.[11] Notably, brown algae's chemical composition changes according to species, habitat, and season.[12]

Heavy metal sorption studies use seaweed-derived sorbents as living (wet) or nonliving (dried and ground) sorbents. In this study, *C. barbata*, which was selected as the biomass, was converted into fibers through electrospinning, increasing its mechanical integrity, hardness, porosity, and thus the performance of biosorption.[13] Electrospinning is a simple and efficient technique used to obtain polymer fiber with diameters ranging from micrometers to submicrons or nanometers using natural and synthetic polymers.[14,15] Electrospun fibers have properties such as tunable porosity, a high surface-to-volume ratio, flexibility in surface functionalities, superior mechanical performance, the ability to control the fiber composition, and the ability to prepare in various sizes and shapes.[16] Due to these advantages, they are preferred in wide areas such as filtration applications, catalysis, cosmetics, energy, protective clothing applications, and sensor technology, in addition to biomedical applications such as wound dressing, tissue engineering, drug delivery, and pharmaceutical composition.[17,18]

Nanofibers have received a lot of attention recently in the field of environmental pollution reduction. Functional polymers with amino, hydroxyl, carboxyl, and sulfhydryl groups can be preferred to fabricate functional nanofibers with good sorption affinity for heavy metals. The ability to alter nanofiber surfaces or combine electrospinning with functional polymers allows them to remove heavy metals from water. Polyacrylonitrile (PAN) is particularly interesting in the sorption of heavy metal ions as its surfaces can be modified to contain various functional groups.[19] Furthermore, PAN is easily electrospinnable and has good mechanical properties, thermal stability, and high chemical resistance. Integrating algae with PAN in a fibrous structure can minimize PAN synthetic polymer usage and fabricate an environmentally friendly product suitable for diverse applications. Großerhode et al.[20] reported that the growth and adhesion of the microalgae *Chlamydomonas reinhardtii* on PAN fibers, and in a recent study, Mantripragada et al.[21] developed that *Chlorella*/PAN nanofibrous membranes for the adsorption of short-chain per- and polyfluoroalkyl substances from water.

In this study, *C. barbata*/PAN biocomposite fiber sorbents were fabricated and then used to remove Pb(II) ions from aqueous media. The morphological, structural, and mechanical properties of the obtained fibers were investigated. To the best of our knowledge, there is no study on using algal-doped polymer biocomposite fibers for heavy metal filtration. This study demonstrated for the first time that *C. barbata* was transformed into a fibrous mat and used as a sorbent for Pb(II). Parameters affecting biosorption were evaluated, encompassing shaking time, algae percentage, pH, biosorbent amount, initial ion concentration, and temperature. The biosorption behavior was comprehensively analyzed utilizing a range of isotherm models, including Langmuir, Freundlich, and Dubinin−Radushkevich, and kinetic models, such as the pseudo-first-order and pseudo-second-order. Postsorption analysis of the fiber sorbent was performed by using SEM/EDS, FTIR, and XPS techniques.

RESULTS AND DISCUSSION

The main aim of this study is to design an algae-doped electrospun fiber and use it as a sorbent material to remove Pb(II) ions from aqueous media for the first time. For this purpose, we prepared fibers by doping brown algae *C. barbata* into PAN by electrospinning, and the sorption ability of the PAN and *C. barbata*/PAN fibers was studied.

Preparation and Characterization of the *C. barbata*/PAN Fibers. The initial step involved the dehydration of raw *C. barbata* using a lyophilizer, followed by grinding and sieving before the electrospinning. Figure 1a−c shows the variations in size, ranging from 3.92 to 49.13 μm with an average diameter of 11.74 ± 1.10 μm. Qualitative determination of elements in the algae sample via EDX spectra (Figure 1d) revealed varying

https://doi.org/10.1021/acsabm.4c00550
ACS Appl. Bio Mater. 2024, 7, 5345−5358

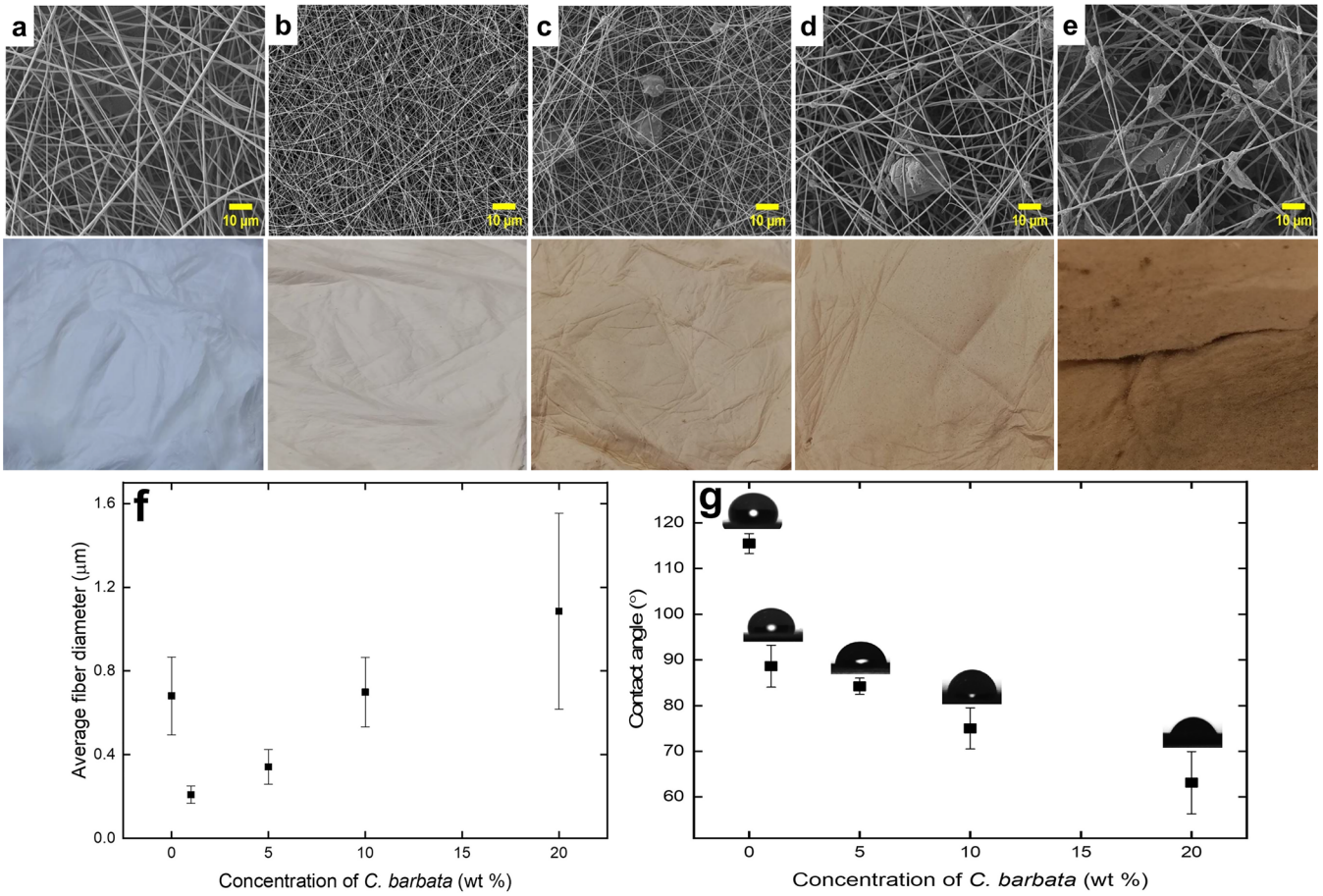

Figure 2. SEM micrographs and photos of *C. barbata*/PAN fibers at different concentrations of *C. barbata*: (a) 0 wt %, (b) 1 wt %, (c) 5 wt %, (d) 10 wt %, and (e) 20 wt %; the relationship between *C. barbata* concentration and (f) average fiber diameter and (g) contact angle (applied voltage: 14 kV, tip-to-collector distance: 19 cm, flow rate: 1 mL h^{-1}, temperature: 25 ± 3 °C, relative humidity: 40 ± 5%).

percentages of C, O, Na, Mg, S, K, and Ca, indicative of environmental influences on *C. barbata* growth conditions. The metal content of the algae sample was quantified using CRM with ICP-MS before its incorporation into the polymer solutions. The raw *C. barbata* utilized in this study exhibited a Pb(II) concentration of 0.585 ± 0.045 mg L^{-1}. The variations in Pb(II) concentrations in *C. barbata* samples collected from diverse regions of the Black Sea and across different seasons are given in Table S2. The variability in metal contents within macroalgae is influenced by factors such as seasonal changes, geographical location, and algae type. Moreover, algae's position, morphological features, age, and environmental conditions in the tidal zone contribute to variations in metal compositions.[22] The disparities in metal concentrations observed in *C. barbata* from the Black Sea are attributed to the specific conditions of the region where the algae grow, coupled with seasonal fluctuations.

The physicochemical properties of electrospinning solutions are known to play an important role in fiber size and morphology during electrospinning of polymeric fibers. The viscosity of the solution is pivotal in determining the concentration range necessary to achieve continuous fibers. A solution with an elevated concentration or viscosity results in the fabrication of larger and smoother fibers. Conversely, lower viscosity leads to the formation of beads or beaded fibers, primarily due to the dominance of surface tension.[14] The physicochemical parameters of electrospinning solutions are given in Table S3. A rise was noted in the electrical conductivity and viscosity values of the formulated PAN solutions, correlating with the concentration and proportionate to the amount of PAN in the solution. Incorporating *C. barbata* into the PAN solution resulted in an initial reduction in solution viscosity, followed by a linear increase corresponding to the rising algae concentration. This phenomenon is believed to be associated with the diminished overall solution viscosity due to the inclusion of a low-viscosity solvent during the preparation of *C. barbata* preparation process. An initial increase (from 1% to 5%) in solution conductivity values was noted upon the addition of algae, followed by a subsequent decrease. The anticipation was that depending on the marine environment supporting the growth of *C. barbata*, the sample would contain salts from its surroundings, thereby elevating the conductivity. Nevertheless, while conductivity tends to increase with biomass at low concentrations, this trend is not mirrored at higher concentrations. This discrepancy is attributed to the limited solubility of the biomass in the solution and its poor electrolyte properties.[23]

SEM micrographs of the fibers obtained from PAN solutions at different concentrations and the concentration-diameter relationship are presented in Figure S2. The average fiber diameter of the PAN fibers were 0.17 ± 0.04 μm (5 wt %), 0.52 ± 0.28 μm (8 wt %), 0.68 ± 0.19 μm (10 wt %), and 0.72 ± 0.30 μm (13 wt %). PAN fibers exhibiting bead-like structures were observed with solutions at 5 and 8 wt %, while

https://doi.org/10.1021/acsabm.4c00550
ACS Appl. Bio Mater. 2024, 7, 5345−5358

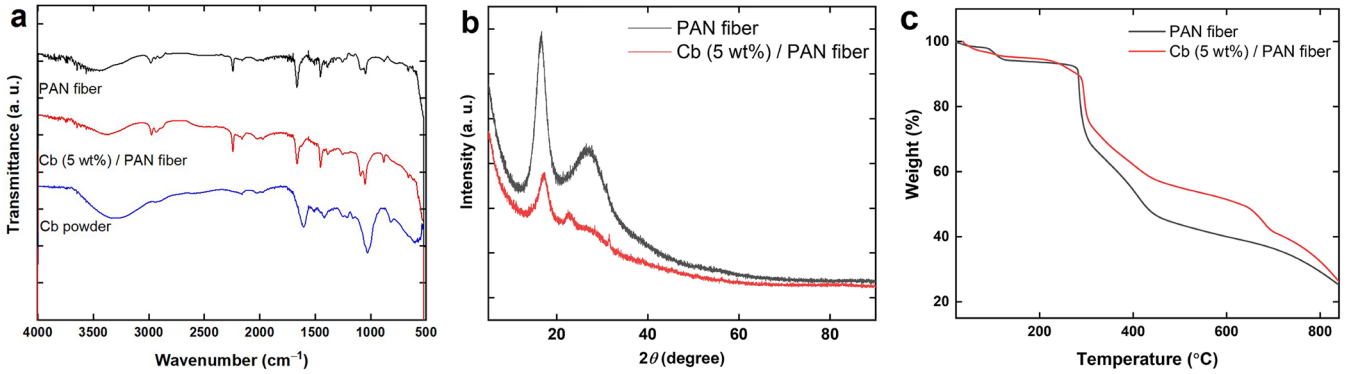

Figure 3. (a) FTIR spectra, (b) XRD pattern, and (c) TGA curve of PAN and *C. barbata*/PAN fibers.

the 13 wt % solution formed discontinuous and thicker fibers. The most regular and homogeneous fiber structures were achieved at a concentration of 10 wt %. The optimum solution concentration is crucial for electrospinning as an increase in concentration corresponds to an increase in fiber diameter. The solution concentration, also related to the viscosity, affects the fabrication of continuous fibers. At lower concentrations, beads form rather than fibers, while higher concentrations hinder the formation of continuous fibers due to the challenge of sustaining the solution flow at the needle tip, leading to the formation of larger fibers.[24]

Figure 2a–e depicts SEM micrographs, photographic images, and average fiber diameter of PAN and *C. barbata*/PAN fibers, illustrating the variations observed with increasing concentrations of *C. barbata* (1, 5, 10, and 20 wt %). Depending on their increasing concentrations, *C. barbata* particles were dispersed in the resulting fibers, and the color of the fiber mats changed from white to brown. In Figure 2(f), the PAN fiber shows a fiber diameter of 0.68 ± 0.19 μm, while the diameters for *C. barbata*/PAN fibers vary with concentrations: 0.21 ± 0.04 μm (1 wt %), 0.34 ± 0.08 μm (5 wt %), 0.70 ± 0.17 μm (10 wt %), and 1.09 ± 0.47 μm (20 wt %). The addition of *C. barbata* initially reduced the fiber diameter, possibly due to the decreased conductivity of the electrospinning solutions. Subsequently, an increase in the fiber diameter of *C. barbata*/PAN was noted, attributed to the higher concentration of *C. barbata* and the resulting increased viscosity of the solutions (see Table S3). We illustrated the extent to which the algae amount could be integrated into the solution, maintaining a constant PAN concentration without interfering with fiber formation, particularly the occurrence of beaded fibers. Hence, *C. barbata* (5 wt %)/PAN fiber exhibiting the most uniform distribution was selected for subsequent characterizations.

EDX spectra and mapping of PAN and *C. barbata*/PAN fibers were analyzed (Figure S3). The distribution of C and N elements inherent to PAN revealed a homogeneous distribution of *C. barbata* along the PAN fibers. Other elements such as C, O, Na, Mg, S, Cl, K, and Ca further confirm the successful fabrication of the *C. barbata*/PAN fibers. The wettability of the fibers was evaluated through contact angle measurements (Figure 2g). PAN fiber exhibited the highest contact angle (115.48 ± 2.16°). However, with an increase in *C. barbata* from 1% to 20% in the PAN fiber, contact angles of the *C. barbata*/PAN fibers decreased (from 88.64 ± 4.59° to 63.13 ± 6.83°), imparting notably enhanced hydrophilic properties. A similar trend in hydrophilicity was observed by Choi et al.[25] for *Spirulina*/PCL nanofibers, where increasing *Spirulina* concentration corresponded to a decrease in contact angles.

Functional groups, including amine, carbonyl, carboxyl, hydroxyl, sulfhydryl, sulfonate, and phosphonate, in the structures of algae, contribute to metal biosorption by different mechanisms.[8] Figure 3a shows FTIR spectra of *C. barbata* powder, PAN, and *C. barbata* (5 wt %)/PAN fibers. Both fibers have a distinctive band of nitrile groups (−C≡N) associated with PAN at 2244 cm^{-1}.[26] The bands in the range of 1450−1000 cm^{-1} are indicative of the C−H (bending) vibration.[27] In the spectrum of *C. barbata* powder, the weak band around 2920 cm^{-1} may be assigned to the $-CH_2$ stretching.[28] Strong asymmetric stretching observed at 1605 cm^{-1}, along with the weak symmetric stretching bands at 1421 cm^{-1}, were linked to carboxylate ions. The presence of these bands resembled those observed in the Ca-alginate-based resin, revealing a substantial presence of alginate in the algal biomass.[29] The band at 1209 cm^{-1} is mainly due to the symmetrical stretching of the $-SO_3$ bonds in the sulfonic acids of polysaccharides, such as fucoidan, commonly present in brown algae. Additionally, the bands at 1030 and 818 cm^{-1} are attributed to the −C−O stretching of the alcoholic and sulfate groups, respectively.[28,29] A broad band is centered at 3300 cm^{-1}, indicative of −OH groups (H-linked alcoholic, carboxylic, and phenolic) in the *C. barbata* powder,[7,29] and this characteristic band was similarly identified in the composite fibers.

Figure 3b shows the XRD patterns of PAN and *C barbata*/PAN fibers. The strong diffraction signal at 2θ = 16.5° corresponds to the crystal plane of the PAN.[30] The weak signal at about 27° is assigned to the amorphous region and rotational disorder in the chain packing.[31] The semicrystalline nature of PAN is attributed to the strong interactions among its nitrile groups.[32] The prominent signal of the *C. barbata*/PAN fiber at about 17° signifies a decrease in crystallinity due to the incorporation of *C. barbata* into the PAN fiber. Additionally, the presence of a signal at 2θ = 22.54° indicates the amorphous structure of *C. barbata*,[33] reducing the crystallinity (56.66% and 36.16% for PAN and *C. barbata*/PAN, respectively).

The thermal stability profiles of both PAN and *C. barbata*/PAN fibers were assessed based on the percentage of weight loss, as depicted in Figure 3c. According to the thermograms, the PAN fiber exhibited no weight loss up to 100 °C, attributed to the cyclization reaction.[34] Initial degradation occurred at around 100 °C, related to moisture and the

https://doi.org/10.1021/acsabm.4c00550
ACS Appl. Bio Mater. 2024, 7, 5345−5358

evaporation of the residue within the polymer. A subsequent PAN fiber degradation occurred at about 280 °C, indicative of functional group separation.[35] In contrast, the *C. barbata*/PAN fiber displayed its initial degradation at around 295 °C, attributed to the improved thermal stability resulting from the algae doping.

The notable features of electrospun fibers, such as high surface area, porosity, and mechanical integrity, were combined with the biosorption ability of *C. barbata*. Sorption operates primarily at the surface level, requiring a sorbent with a considerable surface-to-volume ratio. Table 1 lists the surface area, pore volume, and pore size characteristics of *C. barbata* and PAN powder, as well as PAN and *C. barbata*/PAN fibers. Upon transforming PAN powder into the fibers, the specific surface area underwent an approximately 4-fold increase, rising from 6.20 to 24.56 $m^2\ g^{-1}$. Similarly, the transformation of *C. barbata* into the composite fibers resulted in a more than 2-fold increase, with the specific surface area rising from 4.00 to 8.77 $m^2\ g^{-1}$. A trend was observed for both fibers, where the BET surface area tends to rise alongside increased pore volume, particularly in the presence of smaller pore sizes. By augmenting the surface area, more binding sites are generated within the sorbent regions, facilitating the straightforward binding of metal ions at the solid−liquid interface during biosorption.[36]

Table 1. Surface Area Properties of PAN and *C. barbata* Powder and PAN and *C. barbata*/PAN Fibers

	BET surface area ($m^2\ g^{-1}$)	pore volume ($cm^3\ g^{-1}$)	pore size (nm)
Cb powder	4.00	0.021	15.42
PAN powder	6.20	0.016	21.39
PAN fiber	24.56	0.142	11.24
Cb (5 wt %)/PAN fiber	8.77	0.034	11.96

Mechanical Properties of the *C. barbata*/PAN Fibers. The mechanical properties can influence the performance of the fibers for effective sorption applications. Tensile tests and Young's modulus were used to assess the structural integrity and durability of the fibers. The stress−strain behavior of the fibers, as depicted in Figure 4, indicates that the incorporation of *C. barbata* (5 wt %) into the PAN fibers reduces their tensile strength.

A similar situation has been observed in examinations involving fibers doped with algae and their constituents.[37,38] This phenomenon is believed to arise from the presence of algae powders dispersed extensively within the fibers, where the applied tensile stress is highly concentrated.[38] Furthermore, a simultaneous increase in Young's modulus was observed along with the reduced tensile strength. In addition, PAN fiber modified with *C. barbata* shows increased stiffness and rigidity due to a higher Young's modulus, indicating enhanced deformation resistance and resulting in lower elongation percentages.

Studies indicate that nanofibers with smaller diameters contribute to an elevated Young's modulus, correlating with the enhanced regularity in their structure.[39,40] Naraghi et al. proposed that PAN nanofibers exhibit an elevated Young's modulus when their diameter is below 300 nm.[41] Similarly, the introduction of *C. barbata* to PAN nanofibers reduced fiber diameter (from 0.68 ± 0.19 to 0.34 ± 0.08 μm), resulting in an approximately 2.5-fold increase in Young's modulus.

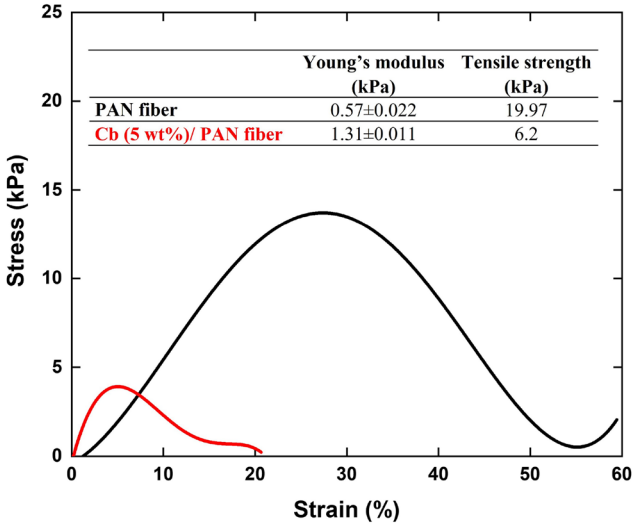

Figure 4. Mechanical testing of the PAN and *C. barbata*/PAN fibers.

Sorption Studies. The biosorption process is influenced by factors such as the characteristics of the biosorbent (surface area, porosity, functional groups) and analyte conditions (pH, temperature, and initial concentration). Additionally, the amount of biosorbent and the contact time are crucial in determining biosorption efficiency.

Effect of Shaking Time. Figure 5a shows the effect of various shaking times and amounts of *C. barbata* in the composite fiber on sorption. The experiments commenced at pH 7 and 25 °C, employing a 10 mL solution with an initial ion concentration of 100.0 $\mu g\ L^{-1}$ and 5 mg of the sorbent. Both the addition of *C. barbata* and the shaking time contributed to an overall enhancement in the sorption capacity of the fibers. The maximum sorption value, achieved at 60 min of shaking time, was 129.68 μg/g (66.54%) using the fiber-containing 5 wt % *C. barbata*. However, a decrease in sorption capacity with the algae concentration occurred upon prolonged exposure of 120 min. It may be due to the desorption of some weakly bound metal ions[36] and the potential aggregation or blocking of active sorption sites by the increasing concentration of algae biomass. This decrease can also be influenced by a reduction in surface area and an increase in pore size, which may lead to fewer available active sorption sites and the presence of larger void spaces within the sorbent material, thereby restricting the accessibility of sorption sites (Table S4).

Sorption Kinetics. Kinetic models offer insights into the sorption process mechanism. The sorption kinetics of Pb(II) ions were evaluated using *C. barbata*-loaded fibers, employing both pseudo-first-order and pseudo-second-order kinetic models. The mathematical equation of the pseudo-first-order model[42] is expressed as eq 1:

$$\ln(q_e - q_t) = \ln(q_e) - k_1 t \quad (1)$$

where q_e and q_t ($mg\ g^{-1}$) are the amounts of Pb(II) sorbed on *C. barbata*/PAN fiber sorbent at equilibrium and time t, respectively. The pseudo-first-order rate constant (k_1, min^{-1}) is determined to establish the representative linear relationship of $\ln(q_e - q_t)$ vs t (Figure S4(a)).

The mathematical equation of pseudo-second-order[42] is given as eq 2:

https://doi.org/10.1021/acsabm.4c00550
ACS Appl. Bio Mater. 2024, 7, 5345−5358

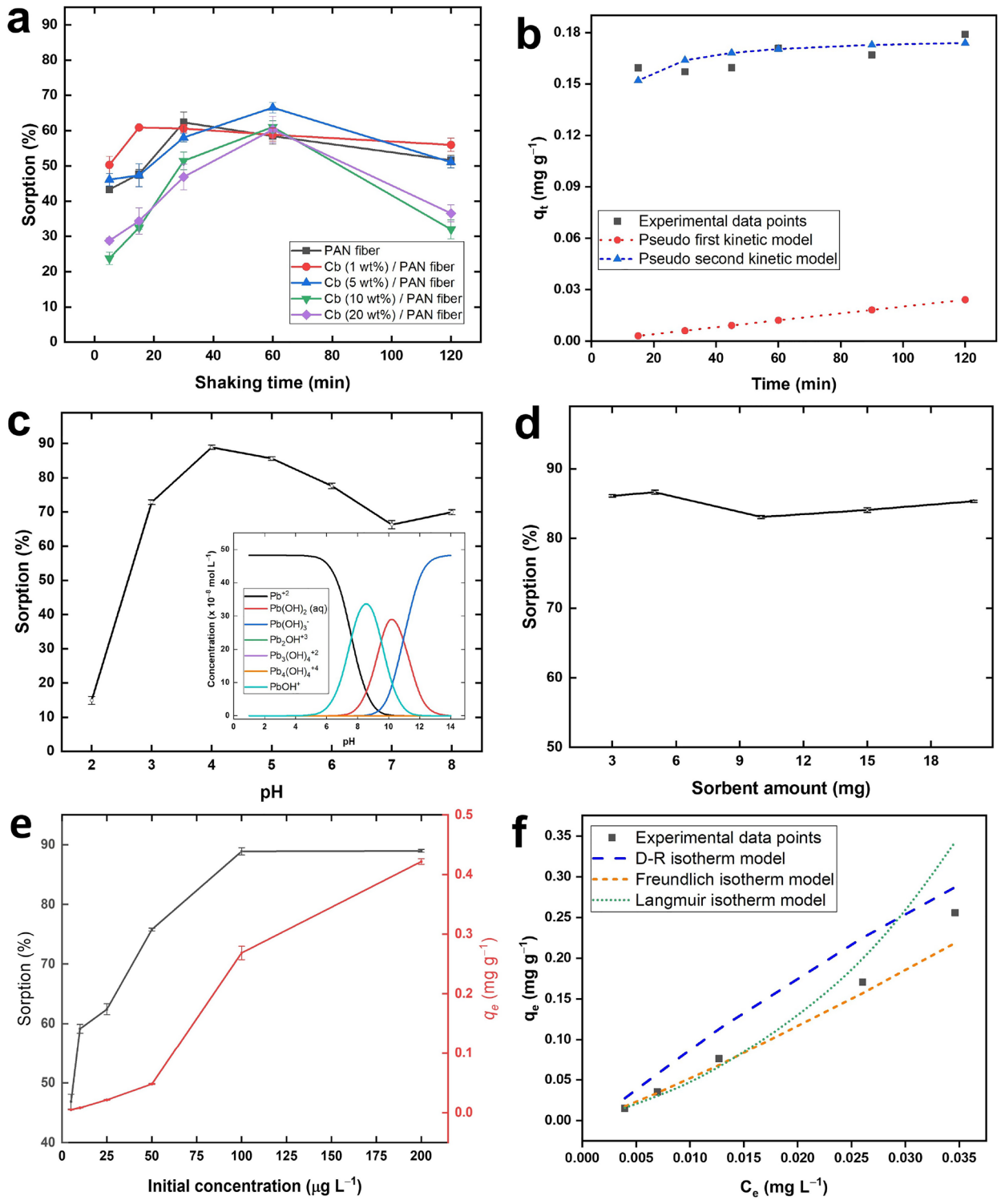

Figure 5. Effect of on the sorption of Pb(II) by *C. barbata*/PAN fibers: (a) shaking time, (b) fitting graphs of adsorption kinetic models, (c) pH (inset figure shows speciation diagram for Pb(II) species), (d) sorbent amount, (e) initial concentration, and (f) fitting graphs of adsorption isotherms models.

$$\frac{t}{q_t} = \frac{1}{k_2 q_e^2} + \frac{1}{q_e} t \qquad (2)$$

where k_2 is the rate constant of the pseudo-second-order at the equilibrium (g mg^{-1} min^{-1}). The values of q_e and k_2 were estimated based on the slope and intercept values of the linear plot of t/q_t vs t (Figure S4(b)).

The parameters influencing sorption kinetics, along with the corresponding correlation coefficient values (R^2) and RMSE, are summarized in Table 2. The pseudo-second-order kinetic model yielded a high correlation coefficient (R^2 > 0.99), suggesting a better fit for describing Pb(II)'s biosorption behavior onto the *C. barbata* (5 wt %)/PAN fiber than the first-order equation. Furthermore, the theoretical value (q_e,

https://doi.org/10.1021/acsabm.4c00550
ACS Appl. Bio Mater. 2024, 7, 5345−5358

Table 2. Kinetic Parameters Derived from Both the Pseudo-First-Order and Pseudo-Second-Order Models for the Biosorption of Pb(II) onto *C. barbata* (5 wt %)/PAN Fiber

kinetic parameters		Pb(II)
experimental	$q_{e,exp}$ (mg g^{-1})	0.1707
pseudo-first-order	R^2	0.8057
	RMSE	0.1533
	$q_{e,calc}$ (mg g^{-1})	1.0168
	k_1 (min^{-1})	3.2×10^{-6}
pseudo-second-order	R^2	0.9962
	RMSE	0.0062
	$q_{e,calc}$ (mg g^{-1})	0.1776
	k_2 (g mg^{-1} min^{-1})	2.2347

calc) aligns well with the experimental data (q_e, exp), indicating that the biosorption process is governed by pseudo-second-order kinetics (Figure 5b). The low RMSE value also supports the reliability of the pseudo-second-order model. The results of the pseudo-second-order kinetic analysis suggest that the biosorption process occurs due to chemical interactions between the metal ions and the binding sites on the sorbent surface.[43]

Effect of pH. The solution pH is an important factor affecting the metal ion species, the dispersed bilayer of the solid−liquid interface, and the sorption process. Furthermore, pH serves as a key determinant in the removal of metal ions from aqueous solutions, impacting factors such as metal ion solubility, the concentration of counterions on the sorbent, the extent of ionization of the sorbate during the reaction, as well as influencing hydrolysis, complexation with organic or inorganic ligands, redox processes, and precipitation phenomena.[44] The pH effect of *C. barbata* (5 wt %)/PAN fiber on the sorption of Pb(II) ions is given in Figure 5c along with the pH-dependent species. pH values were investigated within the range 2.0 to 8.0. The initial Pb(II) concentration was set at 100 μg L^{-1}, and the shaking time was standardized at 60 min. The maximum sorption of the Pb(II) metal occurred at pH 4.0, reaching 88.89%. At this pH, Pb^{2+} exists predominantly, while at pH 5.0 and beyond, Pb hydroxide species begin to form. This finding aligns with the observations made in the metal sorption study involving *C. barbata* by Yalçín et al., where it was reported that the optimal pH range for Pb(II) ions was between 2.5 and 5.0.[7]

Different functional groups (e.g., hydroxyl, carboxyl, and sulfonate groups present in algae cell wall components) are involved in selective metal ion binding, depending on the solution pH.[3] These groups participate according to the dissociation constant (pK_a), responsible for electrostatic interactions with metal ions and creating a negative charge on the algae surface.[45] The sulfonic acid groups (R−S(=O)$_2$−OH) of fucoidan found in brown algae participate in the binding of cations, even at very low pH values, within a pH range where the functionality is most active (typically pK_a values ranging from 1.0 to 2.5). The carboxylic acid groups (R−COOH) of alginic acid undergo changes in their reactivity within the pH range between 3.0 and 5.0. On the other hand, hydroxyl groups (R−OH) are implicated in the metal ion sorption at very high pH values, demonstrating enhanced functionality around a pK_a value of approximately 10.0. Since sorption is avoided at high pH values that cause algae damage and metal precipitation, metal uptake of brown algae is primarily provided with alginate and fucoidan content.[3]

Effect of Sorbent Amount. The sorption efficiency of Pb(II) by *C. barbata* (5 wt %)/PAN at different sorbent amounts (3−5−10−15−20 mg) is depicted in Figure 5d. The experiments were performed at an initial concentration of 100.0 μg L^{-1}, pH 4.0, and 25 °C. The maximum sorption of Pb(II) (86.66%) was observed for 5 mg of the sorbent. At the outset, the initial rise in the amount of sorbent increased the sorption percentage of Pb(II) ions. However, a slight decrease in sorption was noted with a higher amount of sorbent. This situation is explained in two ways: First, during the electrospinning process, the fibers tend to disperse randomly, forming independent fibers. Second, prolonged shaking causes the fibers to coalesce into bundles. This coalescence results in a reduction of the surface/volume ratio within the system. Consequently, a higher barrier is created against the sorption of ions, leading to a decrease in the sorption percentage.[36]

Figure 5e shows the effect of the initial concentration of Pb(II) ions (5.0−10.0−25.0−50.0−100.0−200.0 μg L^{-1}) on the sorption behavior with all other parameters and conditions held constant. The results showed an almost linear increase with the initial Pb(II) concentrations. When the sorption curve

Table 3. Removal of High Concentrations of Pb(II) Ions Using Various Composite Fiber Sorbents at Room Temperature

		sorption parameters						
sorbent	sorption percentage (%)	shaking time (min)	pH	sorbent amount (mg)	initial ion concentration (mg L^{-1})	volume (mL)	sorption isotherms	ref
HEMA modified cellulose	67	180	5.0	100	30	20	Langmuir (R^2: 0.999); Freundlich (R^2: 0.995)	4
PVA/chitosan	84	60	6.0	25	400	10	Langmuir (R^2: 0.915); Freundlich (R^2: 0.894)	46
PVA/PAA	58	120	4.0	100	1	1000	Langmuir (R^2: 0.999); Freundlich (R^2: 0.871)	47
PAN/SL CNF	63	240	5.0−6.0	25	100	250	Langmuir (R^2: 0.999); Freundlich (R^2: 0.990)	48
PVPT/PCL	97	30	8.0	50	10		Langmuir (R^2: 0.970); Freundlich (R^2: 0.980); Dubinin−Radushkevich (R^2:0.934)	49
CA/HAp	99.7	35	6.0	100	10	50	Langmuir (R^2: 0.996); Freundlich (R^2: 0.986)	50
maleate/PAN	98.5	60	6.0	92.5	25	50	Langmuir (R^2: 0.99); Freundlich (R^2: 0.97); Dubinin−Radushkevich (R^2: 0.83)	51
PVDF/AOPAN	99	90	6.0	50	10	20	Langmuir (R^2: 0.997); Freundlich (R^2: 0.842); Redlich−Peterson (R^2: 0.969)	52
Hal-NH_2/CS/PVA	84	120	5.5		450		Langmuir (R^2: 0.996); Freundlich (R^2: 0.944)	53
CA/P-CNFs	80	1	7.0	2	1	50	Langmuir (R^2: 0.994); Freundlich (R^2: 0.871)	54

https://doi.org/10.1021/acsabm.4c00550
ACS Appl. Bio Mater. 2024, 7, 5345−5358

Table 4. Removal of a Low-Concentration Pb(II) Ion with Different Sorbents at Room Temperature

sorbent	sorption percentage (%)	sorption parameters: shaking time (h)	pH	sorbent amount (mg)	initial ion concentration (μg L^{-1})	volume (mL)	sorption isotherms	ref
SPES containing *Eucommia ulmoides*/ PES	85−88	2	7.0	25	200	10	Langmuir (R^2: 0.997); Freundlich (R^2: 0.996)	55
Bauxite, powder	>90	48		250	100	250	Langmuir (R^2: 0.999); Freundlich (R^2: 0.998)	56
C. barbata/PAN fiber	88.89	1	4.0	5.0	100	10	Langmuir (R^2: 0.979); Freundlich (R^2: 0.984); Dubinin− Radushkevich (R^2: 0.998)	this study

Table 5. Isotherm Parameters Obtained by Linear Regression Modeling and Thermodynamic Parameters for Pb(II) Biosorption onto the *C. barbata*/PAN Fiber

isotherm model	parameters			
Langmuir	q_m	K_L	R^2	RMSE
	−0.2062	−18.0310	0.9794	0.5702
Freundich	K_F	n	R^2	RMSE
	10.9330	0.8598	0.9839	0.0422
Dubinin−Radushkevich	E	q_s	R^2	RMSE
	2.32×10^{-8}	1.1871	0.9978	0.0486
thermodynamic parameters	$\Delta G°$ (kJ mol^{-1})		$\Delta H°$ (kJ mol^{-1})	$\Delta S°$ (J K^{-1} mol^{-1})
	298 K	323 K		
	−7.76	−4.5	−46.58	−130.29

reached 100.0 μg L^{-1}, indicating saturation of the sorbent, the sorption percentage was determined to be 88.89% ± 0.63, while at 200.0 μg L^{-1}, it remained nearly unchanged at 88.97% ± 0.27. Sorption capacities were calculated as 270 μg/g ± 11.27 and 420 μg/g ± 4.75, respectively.

The sorption parameters of fiber sorbents prepared with biodegradable materials for Pb(II) removal are given in Table 3. Various composite fibers include PVA/Chitosan, HEMA-modified cellulose, PVA/PAA, PAN/Sago lignin, and PEO/alginate used for Pb(II) sorption. However, it is important to note that the sorption studies listed in the table were conducted using high concentrations of Pb(II) ions (mg L^{-1}). Due to the inherent difficulty in removing heavy metals at low concentrations (μg L^{-1}), there are limited studies available, as indicated in Table 4. Nevertheless, the comparative data support the effectiveness of the *C. barbata*/PAN fiber as a promising sorbent for Pb(II) metal ion removal from aqueous media, as demonstrated in this study.

Sorption Isotherms and Thermodynamics. For sorption isotherm studies, the experimental parameters encompassed a pH of 4.0, a shaking duration of 60 min, a temperature of 25 °C, a sorbent amount of 5 mg, and a varied initial concentration of Pb(II) ions ranging from 10 to 200 μg L^{-1}. Plots of experimental equilibrium data of Pb(II) ions on the *C. barbata* (5 wt %)/PAN fiber with Langmuir, Freundlich, and D-R isotherm models are shown in Figure 5f. Freundlich and Dubinin−Radushkevich isotherms were identified as more fitting, while the Langmuir model proved to be unsuitable for the observed data. The linear plots of the isotherm models with the experimental data for the sorption of Pb(II) ions onto the fiber sorbent are shown in Figure S5. The results for the linearized isotherm models, the regression coefficients (R^2), and the specific parameters are listed in Table 5. The best-fit models were in the following order: Dubinin−Radushkevich (R^2 = 0.9978) > Freundlich (R^2 = 0.9839) > Langmuir (R^2 = 0.9794).

The Langmuir isotherm demonstrates limitations, relying on the assumption of monolayer adsorption of metal ions onto the sorbent surface with a constant system energy. Despite a high R^2, the negative slope and Langmuir isotherm constant indicate its inadequacy in explaining this adsorption process.[57,58] In addition, the fundamental properties of the linearized Langmuir isotherms can be explained in terms of a dimensionless separation factor (R_L) for the equilibrium parameter,[59] which is expressed in eq 3:

$$R_L = \frac{1}{1 + K_L C_0} \tag{3}$$

where C_0 is the initial Pb(II) concentration (mg L^{-1}) and K_L is the Langmuir constant that indicates the nature of sorption (L mg^{-1}). R_L was assessed to see if the adsorption is favorable over the entire range of concentrations, further explaining the fit of the linearized Langmuir model. The presence of negative values (R_L < 0) in the linearized Langmuir equations implies inadequacy of the equations.[57,59] The R_L values for the Langmuir model range from −0.9349 to −0.2794 for the initial concentrations of 100 to 200 mg L^{-1} (Table 5). The trend of increasing R_L values with higher initial concentrations implies potential favorability in the adsorption of Pb(II) ions. However, the negative R_L values obtained in this case indicate that the Langmuir isotherm is not a suitable model for describing the favorable adsorption of Pb(II) ions.[57]

The Freundlich sorption capacity (K_F) represents the maximum adsorption capacity. On the other hand, the adsorption density (n) characterizes the intensity of adsorption and the nature of the adsorption process. Adsorption is considered promising if the K_F value falls within the range of 1−20, and the n value exceeds 1.[60] A K_F value of 10.9330 and an n value of 0.8598 (Table 5) collectively suggest nuanced adsorption behavior with a substantial adsorption capacity and a preference for lower concentrations, respectively. This may

https://doi.org/10.1021/acsabm.4c00550
ACS Appl. Bio Mater. 2024, 7, 5345−5358

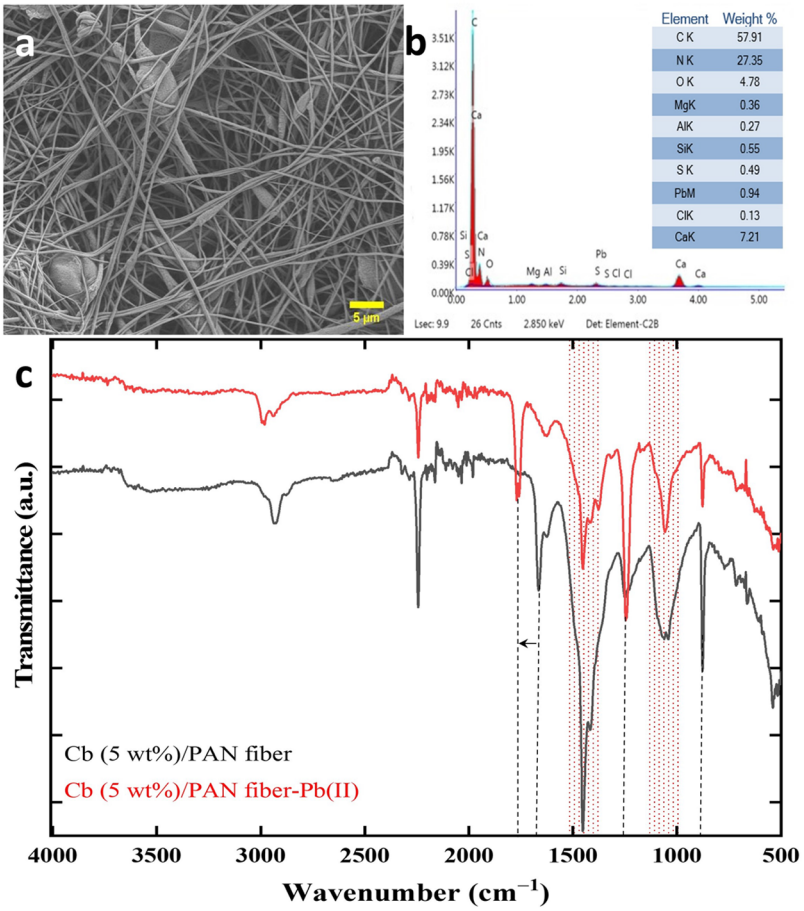

Figure 6. (a) SEM micrograph, (b) EDX spectrum, and (c) FTIR spectra of the *C. barbata*/PAN fibers after Pb(II) sorption.

also indicate the possibility of multilayer adsorption or heterogeneous surfaces.[61]

The Dubinin−Raduskevich (D-R) model provides important insight into whether the adsorption mechanism is physical or chemical.[62] This is determined by the D-R characteristic energy (E) value (eq 4), indicating physical interactions such as electrostatic or hydrogen bonding between the sorbent and metal ions.[62] The sorption is categorized as physical when the E number is between 1 and 16 kJ mol^{-1} and as chemisorption when it is greater than 16 kJ mol^{-1}.[61] Table 5 shows that the computed value of E is 4.64 kJ mol^{-1}, indicating that Pb(II) ion sorption onto the fiber sorbent through physical interactions. In addition, the D-R isotherm model outperforms the Langmuir isotherm model due to its exclusion of assumptions regarding a homogeneous surface or constant adsorption potential.[60]

$$E = \frac{1}{\sqrt{-2K_D}} \tag{4}$$

In addition to the isotherm curves given in Figure 5f, all isotherm models seem to be suitable for the experimental data regarding R^2 values. On the other hand, Pb(II) sorption can be explained by both Freundlich and Dubinin−Radushkevich due to high R^2 values and low RMSE values (Table 5), indicating that the adsorption mechanism has a heterogeneous structure.[63]

Table 5 also lists the thermodynamic parameters for Pb(II) biosorption onto the fiber, providing information about the type and mechanism of the sorption process. A negative value of the enthalpy change ($\Delta H°$; −46.58 kJ mol^{-1}) indicates that the sorption of Pb(II) ions onto the fiber sorbent is exothermic. These results are consistent with our experimental results, as the Pb(II) ion sorption percentage decreases with temperature (88.89% ± 0.63−71.07% ± 0.34). On the other hand, a negative value of entropy change ($\Delta S°$) represents decreased randomness at the solid-solution interface during the sorption process, which can be indicative of specific binding sites, surface interactions without substantial changes in the sorbent structure.[64] Furthermore, a negative value of Gibbs free energy ($\Delta G°$) indicates the feasibility and spontaneous nature of the Pb(II) ion sorption process.[64] However, with an increase in temperature, the magnitude of $\Delta G°$ rises, leading to a less favorable scenario for the sorption.

Postsorptive Sorbent Characterization. Morphological and structural postsorptive characterization of the sorbent is crucial for a comprehensive understanding of the sorption mechanism. Figure 6a,b shows the SEM micrograph and EDX analysis of the used *C. barbata* (5 wt %) /PAN fiber. The fibrous structure of the sorbent was retained even after the sorption of Pb(II) ions, and elemental analysis evidenced the presence of Pb(II) ions on the fiber sorbent. Figure 6c illustrates the changes in the FTIR spectrum after sorption, confirming the attachment of the Pb(II) ions to the fiber surface.

Accordingly, the interaction of Pb(II) ions with the composite fibers was mainly reflected by the blue shift in the stretching vibration of the asymmetric C═O band (from 1661 to 1760 cm^{-1}), and the decrease in the symmetric C═O vibration at 1450 cm^{-1}, while the C−O band at 1060 cm^{-1}

https://doi.org/10.1021/acsabm.4c00550
ACS Appl. Bio Mater. 2024, 7, 5345−5358

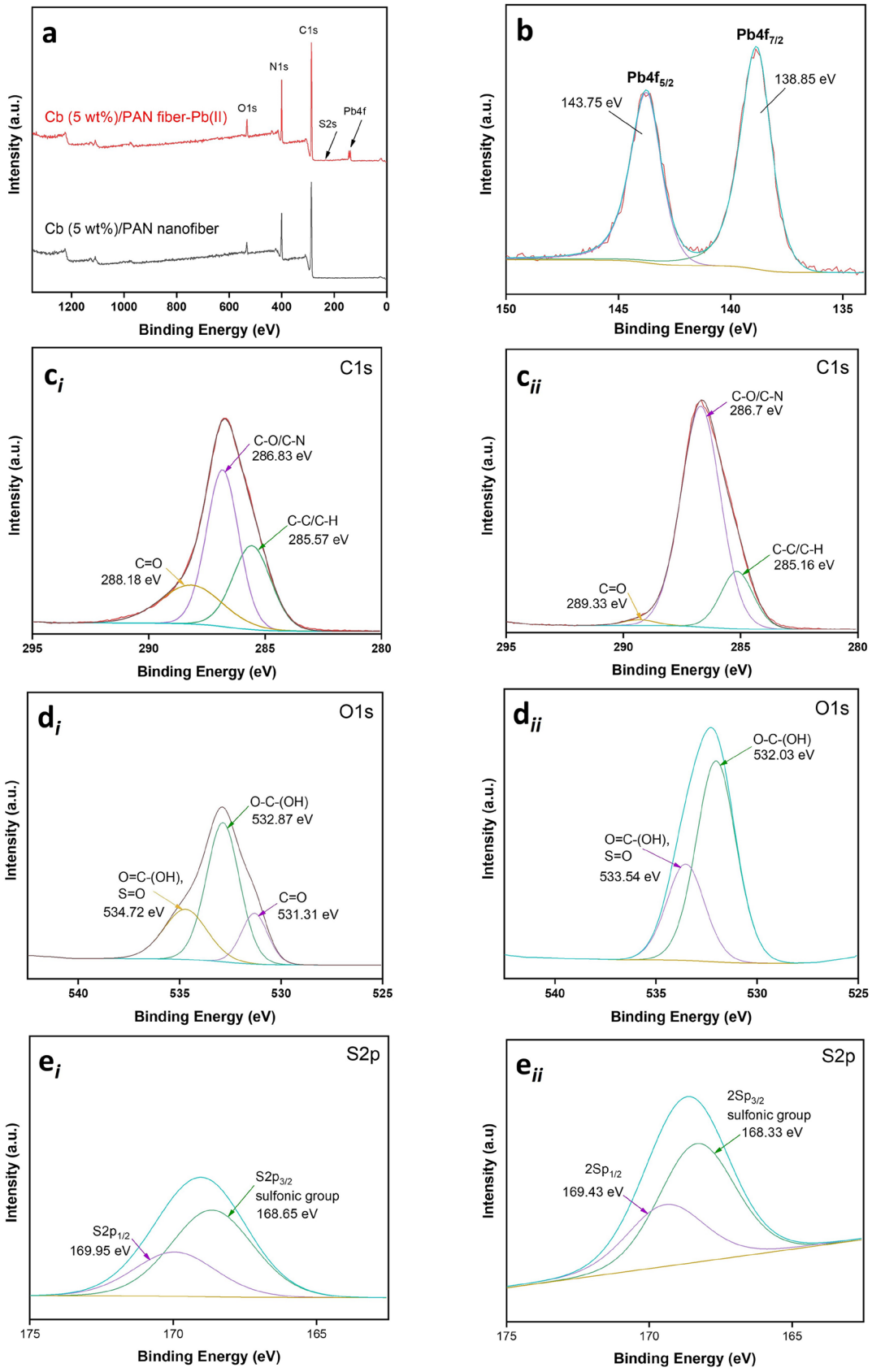

Figure 7. XPS analysis of the *C. barbata*/PAN fibers before and after Pb(II) sorption. (a) A wide scan survey and deconvoluted spectra of (b) Pb 4f, (c_i and c_{ii}) C 1s, (d_i and d_{ii}) O 1s, (e_i and e_{ii}) S 2p. The subscripts *i* and *ii* indicate the state before and after sorption, respectively.

became apparent. Furthermore, changes were observed in the vibrational modes of the sulfonic acid groups upon sorption, accompanying an increase in the asymmetric and symmetric $-SO_3$ stretching bands at 1372 and 1243 cm^{-1}, respectively,

https://doi.org/10.1021/acsabm.4c00550
ACS Appl. Bio Mater. 2024, 7, 5345−5358

and a decrease in the S=O stretching band at 874 cm^{-1}. The contribution of carboxyl groups of the alginate and sulfonate groups of fucoidan to heavy metal biosorption has been reported in the literature.[7,28,65]

XPS analysis was performed to elucidate the Pb(II)−adsorbent interactions by examining the binding energies of the relevant species. Figure 7a shows a wide survey of the fiber sorbents before and after Pb(II) sorption. The signals arise from the backbone of PAN and *C. barbata*, namely, C, N, O, and S. Upon sorption, the detection of Pb 4f confirms the presence of Pb(II) on the surface of the fiber sorbent. The Pb 4f profile in Figure 7b revealed prominent signals at 143.75 and 138.85 eV, corresponding to Pb $4f_{5/2}$ and Pb $4f_{7/2}$, respectively. The Pb $4f_{7/2}$ signal can indeed be associated with various chemical species, including $-COOPb^+$, $(-COO)_2Pb$, and $-OPb^+$, as mentioned in the study by Liang et al.[66] Functional groups, such as carboxyl and hydroxyl, indicate that these groups are active as electron donors in the sorption of Pb(II) ions onto the fiber.

C 1s XPS spectra of the *C. barbata*/PAN nanofiber exhibited peaks at binding energies of 285.57, 286.83, and 288.18 eV, which can be attributed to C−C/C−H, C−O/C−N, and C=O, respectively, thereby confirming the incorporation of *C. barbata* within the fiber (Figure 7c_i). After sorption, the observed shift of C=O to a higher binding energy may be attributed to the coordination of Pb(II) with C=O groups, thereby reducing their carboxyl character and predominantly converting into C−O bonds (Figure 7c_{ii}). Similarly observed in the O 1s profile, the peak associated with C=O at 531.31 eV disappeared completely, while the two peaks at 534.72 and 532.87 eV (Figure 7d_i) shifted to 533.54 and 532.03 eV, respectively (Figure 7d_{ii}). It is also evident that changes in the electron distribution of oxygen atoms in the environment may occur due to the formation of bonds between Pb(II) ions and oxygen atoms, complexation with hydroxyl groups, and ion exchange reactions with carboxylate groups. Furthermore, the increase in the peak area after sorption can also be attributed to S=O originating from the sulfonic acid groups of fucoidan in the *C. barbata* biomass, contributing to Pb(II) sorption.[67,68] This finding is further supported by the alterations observed in the S 2p spectra (Figure 7e_i and e_{ii}), which are deconvoluted into two peaks (S $2p_{3/2}$ and S $2p_{1/2}$), attributed to $-SO_3H$ groups.[68] Upon sorption, both peaks shifted to lower binding energies. This harmonious shift, which occurs almost without a significant change in the area, is an indicator of the change in electron distribution in the oxygen groups to which the sulfur atoms are attached.

EXPERIMENTAL SECTION

Materials. Polyacrylonitrile (PAN, M_w = 150000 g mol^{-1}) and *N*,*N*-dimethylformamide (DMF) were purchased from Sigma-Aldrich, Germany. Lead(II) nitrate ($Pb(NO_3)_2$) was supplied by Merck, Germany. Nitric acid (HNO_3, 64−66% Sigma-Aldrich, Germany) and ammonia solution (NH_3, 25% Merck, Germany) were used for pH adjustment. The chemicals were of analytical grade, and all aqueous solutions were prepared with ultrapure water (electrical conductivity = 0.05 μS/cm).

Algae Preparation. *Cystoseira barbata*, a marine brown algae (Phylum: Ochrophyta, Class: Phaeophyceae, Order: Fucales, Family: Sargassaceae), was collected in the upper infralittoral zone from the coastal region of Hamsilos (Sinop, Turkey; 42° 3′ 38.4″ N; 35° 2′ 40.4″ E) in August 2020, at the depth 0−3 m. Freshly collected algae were washed with tap water to remove salt, sand, epiphytes, and other marine organisms and then washed several times with distilled water. Freeze-drying of algae was done using a freeze-dryer (XQ-Instrument freeze-dry/XQ-12B) at −40 °C, working pressure of 1 Pa for 72 h. Dried *C. barbata* was milled with a ring mill (Retsch RS 200) and sieved at ∼100 μm. Different sizes of *C. barbata* of images were acquired by a stereo microscope (Olympus, SZX7). The *C. barbata* powder was stored at −20 °C until used.

Electrospinning. The electrospinning solution of PAN was prepared with different concentrations (5, 8, 10, and 13 wt %) by dissolving the polymer in DMF. The solutions were stirred at room temperature for 24 h until homogeneous.[19] The concentrations of *C. barbata* in the 10 wt % PAN solution were added as 1, 5, 10, and 20 wt %. Algae dispersed in an ultrasonic bath for 1 h, then homogenized by mixing for 5 h. The solutions of PAN and *C. barbata*/PAN were filled in a 10 mL syringe. The syringe was attached to the metal needle tip with an inner diameter of 0.2 mm and was fixed horizontally on the micro syringe pump. The PAN and *C. barbata*/PAN fibers were obtained using electrospinning (Inovenso Basic Set-up). The electrospinning process conditions were as follows: flow rate is 1 mL h^{-1}, voltage is 14 kV, and distance between the needle tip and collector is 19 cm.[19] The process was conducted at 25 ± 3 °C and 40 ± 5% humidity for 2 h.

Characterization of Algae and Electrospun Fibers. The metal concentration of *C. barbata* was measured by inductively coupled plasma mass spectrometry (ICP-MS, Agilent 7800) after the algae sample was mineralized with a microwave digestion system (Milestone ETHOS EASY). The accuracy of the analyses was checked using certified reference material (CRM-BCR-279, Sea Lettuce (*Ulva lactuca*)). The surface morphology of *C. barbata* and electrospun fibers were analyzed by scanning electron microscope (SEM Carl Zeiss 300 VP) equipped with an energy-dispersive X-ray (EDX) detector after the gold coating. Element distributions on the micrographs were obtained with EDX elemental mapping. The average fiber diameters (AFD) were evaluated from approximately 100 randomly selected fibers on SEM micrographs by using the ImageJ software. The water contact angles of the fibers were measured with a KSV Attension Theta Optical Tensiometer. Fourier transform infrared spectra were acquired using an FTIR spectrometer (Thermo Fisher Scientific, 105 ATR and PerkinElmer Spectrum Two FT-IR) to examine functional groups of *C. barbata* and fibers. The thermal properties of the fibers were conducted using a TGA-SDT Q600 thermogravimetric analyzer. X-ray diffraction (XRD) patterns were collected by a Philips X'Pert Pro diffractometer. The surface area and pore size distribution of the fibers were determined by a Brunauer−Emmett−Teller (BET, Micromeritics 3Flex) analyzer using the nitrogen adsorption method. The superficial composition of *C. barbata*/PAN nanofibers was analyzed using X-ray photoelectron spectroscopy (XPS) employing a monochromatic energy source (Al Kα radiation, 1486.6 eV) with the Thermo Scientific K-Alpha instrument.

Mechanical Properties of Fibers. The tensile tests of the fibers were conducted using universal tensile testing equipment (Shimadzu AGS-X) with a load capacity of 5 kN to determine their mechanical properties. The tests were conducted at the tension speed of 10 mm/min and ambient temperature (n = 3).[69] The size of the samples was 45 × 30 mm (length × width), and the thickness was 90−250 μm (the thicknesses used for the calculation were measured individually for each sample; Figure S1a−d). The fiber thicknesses were measured by scaling stereo microscope images taken at various points (Olympus, SZX7).

Biosorption Studies. Batch trials were carried out to evaluate the biosorption efficiency of the *C. barbata*/PAN fiber for Pb(II). A thermostat-controlled water bath (GFL 1083) was used, and the solutions underwent stirring at 1000 rpm. The stock solution (1000 mg L^{-1}) of Pb(II) was prepared by dissolving the Pb salt in ultrapure water. By diluting the stock solution, the standard solutions of Pb(II) with different concentrations (5, 10, 25, 50, 100, 200, 500, and 1000 μg L^{-1}) was obtained. All solutions were acidified with HNO_3 (1% v/v) and were stored in the refrigerator at 4 °C. The effects of biosorption parameters such as initial metal ion concentration (5, 10, 25, 50, 100, and 200 μg L^{-1}), pH (2.0, 3.0, 4.0, 5.0, 6.0, 7.0, and 8.0),

https://doi.org/10.1021/acsabm.4c00550
ACS Appl. Bio Mater. 2024, 7, 5345−5358

shaking time (5, 15, 30, 60, and 120 min), sorbent amount (3, 5, 10, 15, and 20 mg), the content of *C. barbata* in the PAN (1, 5, 10, and 20 wt %), and temperature (25 and 50 °C) on the removal of Pb(II) ions were studied. The residual concentration in the solution was measured by ICP-MS, and the instrument operating parameters were presented in Table S1. The biosorption percentage and capacity were calculated using the following eqs 5 and 6, respectively:

$$\text{biosorption}(\%) = \left(\frac{C_i - C_f}{C_i}\right) \times 100 \tag{5}$$

$$q_e(\text{mg g}^{-1}) = \left(\frac{C_i - C_f}{W}\right) \times V \tag{6}$$

where C_i and C_f represent the initial and final concentrations of Pb(II) ions, and W and V denote the mass of sorbent and the volume of the analyte, respectively. The speciation diagram of Pb(II) ions at different pH levels was constructed by using Visual MINTEQ software.

To evaluate the relationship between the equilibrium concentration of sorbate in bulk and the amount sorbed at the fibrous surface, different isotherm models, including Langmuir, Freundlich, and Dubinin−Radushkevich, were applied. The linear form of the Langmuir isotherm model is written as the following eq 7.[27]

$$\frac{1}{q_e} = \left(\frac{1}{K_L q_m}\right) \times \frac{1}{C_e} + \frac{1}{q_m} \tag{7}$$

According to the linear fits of Pb(II) ions on the *C. barbata*/PAN fiber sorbent (Figure S5), Langmuir isotherm parameters were obtained using the graph between $1/q_e$ and $1/C_e$.

Similarly, Freundlich isotherm parameters were calculated using the plot between log q_e and log C_e, depending on the eq 8:[27]

$$\log q_e = \log K_F + \frac{1}{n} \log C_e \tag{8}$$

C_e is the equilibrium metal ion concentration (mg L^{-1}), q_e is the equilibrium biosorption capacity (mg g^{-1}), q_m is the maximum biosorption capacity (mg g^{-1}), K_F and n are Freundlich isotherm constants, K_F is an indicator of biosorption capacity, and K_L is the Langmuir constant related to the energy of biosorption, L mg^{-1}. Likewise, the relative parameters of the Dubinin−Radushkevich isotherm[62] were also determined from the plots of ln q_e vs ϵ^2, applying eqs 9 and 10:

$$\ln q_e = \ln q_s - K_D \epsilon^2 \tag{9}$$

$$\epsilon^2 = RT \ln\left(1 + \frac{1}{C_e}\right) \tag{10}$$

q_s (mg g^{-1}) is a constant in the Dubinin−Radushkevich isotherm model related to biosorption capacity and K_{DR} (mol^2 kJ^{-2}) is a constant associated with the mean free energy of biosorption. ϵ (kJ mol^{-1}) is the Polanyi potential, R is the universal gas constant (8.314 J mol^{-1} K^{-1}), and T is the temperature (K).

The agreement of the plot obtained from isotherm and kinetic data was evaluated by the Root Mean Square Error (RMSE) in eq 11.[70]

$$\text{RMSE} = \sqrt{\frac{1}{N}\sum_{i=1}^{n}(X_{exp} - X_{cal})} \tag{11}$$

To investigate the effect of temperature on Pb(II) biosorption, the experiments were carried out at 25 and 50 °C. Using the data obtained, the thermodynamic parameters such as standard Gibbs free energy change ($\Delta G°$), enthalpy change ($\Delta H°$), and entropy change ($\Delta S°$) were calculated by the following equations.[64]

$$\Delta G° = -RT \ln K_c \tag{12}$$

$$\Delta G° = \Delta H° - T\Delta S° \tag{13}$$

The linear form of the Van't Hoff equation (eq 14) can be obtained by combining eqs 12 and 13:

$$\ln K_c = \frac{\Delta S°}{R} - \frac{\Delta H°}{RT} \tag{14}$$

where R (8.314 J mol^{-1} K^{-1}) is the ideal gas constant and T (K) is the temperature. The slope and intercept of the Van't Hoff plot, i.e., as the linear plot of ln K_c versus $1/T$, give $\Delta H°$ and $\Delta S°$, respectively.[64]

CONCLUSION

The electrospinning of PAN fibers doped with *C. barbata* for removal of Pb(II) from waters was successfully achieved. The conversion of *C. barbata* powder into fibers has an increased surface area, enhancing the availability of metal binding sites during the sorption process. The maximum sorption percentage of the *C. barbata* (5 wt %)/PAN fibers for Pb(II) was (89−90%) at pH 4.0 and an initial concentration of 100 μg L^{-1}, after 60 min. When the R^2 and RMSE values are considered together, the equilibrium data fit well with the Freundlich and Dubinin−Radushkevich isotherm model, while the pseudo-second-order kinetic model offers the best description of the sorption. Postsorption characterization revealed that the carboxyl, hydroxyl, and sulfonyl groups provided by algae doping played active roles in Pb(II) sorption. *C. barbata*/PAN fiber emerged as a low-cost, practical, and environmentally friendly sorbent for removing Pb(II) ions, demonstrating promising potential in water treatment applications. Furthermore, addressing the removal of heavy metals at low concentrations is crucial for mitigating potential environmental hazards and safeguarding human health, as even trace amounts of these contaminants can accumulate over time and pose significant risks to ecosystems and organisms.

ASSOCIATED CONTENT

Data Availability Statement

Data will be made available on request.

Supporting Information

The Supporting Information is available free of charge at https://pubs.acs.org/doi/10.1021/acsabm.4c00550.

Supplementary data associated with this article (PDF)

AUTHOR INFORMATION

Corresponding Author

Nesrin Horzum − *Department of Engineering Science, Faculty of Engineering and Architecture, İzmir Katip Çelebi University, İzmir 35620, Turkey;* orcid.org/0000-0002-2782-0581; Email: nesrin.horzum.polat@ikcu.edu.tr

Authors

Fatma Rabia Karaduman − *Graduate School of Natural and Applied Sciences, İzmir Katip Çelebi University, İzmir 35620, Turkey;* orcid.org/0000-0001-7317-3445

Saniye Türk Çulha − *Department of Basic Science, Faculty of Fisheries, İzmir Katip Çelebi University, İzmir 35620, Turkey;* orcid.org/0000-0003-0380-0858

Complete contact information is available at: https://pubs.acs.org/10.1021/acsabm.4c00550

Notes

The authors declare no competing financial interest.

https://doi.org/10.1021/acsabm.4c00550
ACS Appl. Bio Mater. 2024, 7, 5345−5358

■ ACKNOWLEDGMENTS

This work was supported by the Scientific Research Projects Coordination Unit of İzmir Katip Çelebi University (Project No: 2020-TDR-FEBE-0013). The Council of Higher Education (CoHE) 100/2000 Ph.D Scholarship supported the study. The authors thank Dr. Ayşegül Ülkü Metin in the Department of Chemistry of the University of Kírıkkale for assistance with sorption kinetics, isotherms, and thermodynamics. The authors also thank Dr. Tarkan Akderya in the Department of Biomedical Engineering of the University of Bakírçay for assistance with the mechanical analysis.

■ REFERENCES

(1) Singh, J.; Yadav, P.; Pal, A. K.; Mishra, V. *Sensors in Water Pollutants Monitoring: Role of Material*; Springer, 2019; pp 5−20.
(2) Qasem, N. A.; Mohammed, R. H.; Lawal, D. U. Removal of heavy metal ions from wastewater: A comprehensive and critical review. *npj Clean Water* **2021**, *4*, 1−15.
(3) Mazur, L. P.; Cechinel, M. A.; de Souza, S. M. G. U.; Boaventura, R. A.; Vilar, V. J. Brown marine macroalgae as natural cation exchangers for toxic metal removal from industrial wastewaters: A review. *J. Environ. Manage.* **2018**, *223*, 215−253.
(4) Gouda, M.; Aljaafari, A. Removal of Heavy Metal Ions from Wastewater Using Hydroxyethyl Methacrylate-Modified Cellulose Nanofibers: Kinetic, Equilibrium and Thermodynamic Analysis. *Int. J. Environ. Res. Public Health* **2021**, *18*, 6581.
(5) Chowdhury, I. R.; Chowdhury, S.; Mazumder, M. A. J.; Al-Ahmed, A. Removal of lead ions (Pb^{2+}) from water and wastewater: a review on the low-cost adsorbents. *Appl. Water Sci.* **2022**, *12*, 185.
(6) Cirik, Y. O.; Buyukates, Y.; Merdivan, M. A comparison of biosorption capacities of *Cystoseira barbata* and *Caulerpa racemosa* using Cd(II) and Co(II) ions. *Fresenius Environ. Bull.* **2014**, *23*, 2016−2026.
(7) Yalçín, S.; Sezer, S.; Apak, R. Characterization and lead (II), cadmium (II), nickel (II) biosorption of dried marine brown macro algae *Cystoseira barbata*. *Environ. Sci. Pollut. Res.* **2012**, *19*, 3118−3125.
(8) Romera, E.; Gonzalez, F.; Ballester, A.; Blázquez, M. L.; Munoz, J. Biosorption with algae: a statistical review. *Crit. Rev. Biotechnol.* **2006**, *26*, 223−235.
(9) Karaduman, F. R.; Çulha, S. T.; Horzum, N. Algal nanofibers: Current status and recent developments. *Mater. Today Commun.* **2022**, *33*, 104248.
(10) Guiry, M. D.; Guiry, G. AlgaeBase. World-wide electronic publication; National University of Ireland, Galway, 2020. https://www.algaebase.org (accessed: 2024−06−28).
(11) Manev, Z. K.; Petkova, N. T. Component composition and antioxidant potential of Cystoseira barbata from the Black Sea. *Bull. Transilv. Univ. Bras. II: For. Wood Ind. Agric. Food Eng.* **2021**, *63*, 163−172.
(12) Chadova, T. V.; Korshenko, L. O.; Smertina, E. S.; Nekrasov, A. E.; Berlova, N. V. Development of a Biodegradable Additive from Brown Algae of the Russian Far East for the Production of Plastic Packaging. *Adv. Syst. Sci. Appl.* **2016**, *16*, 47−61.
(13) Dodson, J. R.; Parker, H. L.; García, A. M.; Hicken, A.; Asemave, K.; Farmer, T. J.; He, H.; Clark, J. H.; Hunt, A. J. Bio-derived materials as a green route for precious & critical metal recovery and re-use. *Green Chem.* **2015**, *17*, 1951−1965.
(14) Bhardwaj, N.; Kundu, S. C. Electrospinning: a fascinating fiber fabrication technique. *Biotechnology Advances* **2010**, *28*, 325−347.
(15) Horzum, N.; Muñoz-Espí, R.; Hood, M. A.; Demir, M. M.; Crespy, D. 2. Green Processes and Green Fibers. *Green Electrospinning*; De Gruyter: Berlin, Germany, 2019; pp 11−40.
(16) Huang, Z.-M.; Zhang, Y.-Z.; Kotaki, M.; Ramakrishna, S. A review on polymer nanofibers by electrospinning and their applications in nanocomposites. *Compos. Sci. Technol.* **2003**, *63*, 2223−2253.
(17) Fang, J.; Niu, H.; Lin, T.; Wang, X. Applications of electrospun nanofibers. *Chin. Sci. Bull.* **2008**, *53*, 2265−2286.
(18) Horzum, N.; Mete, D.; Karakuş, E.; Üçüncü, M.; Emrullahoğlu, M.; Demir, M. M. Rhodamine-immobilised electrospun chitosan nanofibrous material as a fluorescence turn-on Hg^{2+} sensor. *ChemistrySelect* **2016**, *1*, 896−900.
(19) Horzum, N.; Shahwan, T.; Parlak, O.; Demir, M. M. Synthesis of amidoximated polyacrylonitrile fibers and its application for sorption of aqueous uranyl ions under continuous flow. *Chem. Eng. J.* **2012**, *213*, 41−49.
(20) Großerhode, C.; Wehlage, D.; Grothe, T.; Grimmelsmann, N.; Fuchs, S.; Hartmann, J.; Mazur, P.; Reschke, V.; Siemens, H.; Rattenholl, A.; et al. Investigation of microalgae growth on electrospun nanofiber mats. *AIMS Bioengineering* **2017**, *4*, 376−385.
(21) Mantripragada, S.; Deng, D.; Zhang, L. Algae-Enhanced Electrospun Polyacrylonitrile Nanofibrous Membrane for High-Performance Short-Chain PFAS Remediation from Water. *Nanomaterials* **2023**, *13*, 2646.
(22) Neshovska, H.; Manev, I.; Kirov, V. Heavy metal levels in water, brown algae (*Cystoseira barbata*), and eelgrass (*Zostera marina*) from the Southern Black Sea coast of Bulgaria. *Int. J. Vet. Sci. Anim. Husb.* **2021**, *6*, 15−18.
(23) de Morais, M. G.; Stillings, C.; Dersch, R.; Rudisile, M.; Pranke, P.; Costa, J. A. V.; Wendorff, J. Preparation of nanofibers containing the microalga *Spirulina* (*Arthrospira*). *Bioresour. Technol.* **2010**, *101*, 2872−2876.
(24) Sukigara, S.; Gandhi, M.; Ayutsede, J.; Micklus, M.; Ko, F. Regeneration of Bombyx mori silk by electrospinning—part 1: processing parameters and geometric properties. *Polymer* **2003**, *44*, 5721−5727.
(25) Choi, J. I.; Kim, M. S.; Chung, G. Y.; Shin, H. S. *Spirulina* extract-impregnated alginate-PCL nanofiber wound dressing for skin regeneration. *Biotechnol. Bioprocess Eng.* **2017**, *22*, 679−685.
(26) Chen, C.; Li, F.; Guo, Z.; Qu, X.; Wang, J.; Zhang, J. Preparation and performance of aminated polyacrylonitrile nanofibers for highly efficient copper ion removal. *Colloids Surf. A: Physicochem. Eng. Asp.* **2019**, *568*, 334−344.
(27) Feng, Q.; Wu, D.; Zhao, Y.; Wei, A.; Wei, Q.; Fong, H. Electrospun AOPAN/RC blend nanofiber membrane for efficient removal of heavy metal ions from water. *J. Hazard. Mater.* **2018**, *344*, 819−828.
(28) Ali, H. S.; Kandil, N. F. E. S.; Ibraheem, I. B. Biosorption of Pb^{2+} and Cr^{3+} ions from aqueous solution by two brown marine macroalgae: an equilibrium and kinetic study. *Desalin. Water Treat.* **2020**, *206*, 250−262.
(29) Sheng, P. X.; Ting, Y.-P.; Chen, J. P.; Hong, L. Sorption of lead, copper, cadmium, zinc, and nickel by marine algal biomass: characterization of biosorptive capacity and investigation of mechanisms. *J. Colloid Interface Sci.* **2004**, *275*, 131−141.
(30) Assaifan, A. K.; Aijaz, M. O.; Luqman, M.; Drmosh, Q.; Karim, M. R.; Alharbi, H. F. Removal of cadmium ions from water using coaxially electrospun PAN/ZnO-encapsulated PVDF nanofiber membranes. *Polym. Bull.* **2022**, *79*, 2831−2850.
(31) Furushima, Y.; Nakada, M.; Takahashi, H.; Ishikiriyama, K. Study of melting and crystallization behavior of polyacrylonitrile using ultrafast differential scanning calorimetry. *Polymer* **2014**, *55*, 3075−3081.
(32) Zhang, H.; Quan, L.; Gao, A.; Tong, Y.; Shi, F.; Xu, L. The structure and properties of polyacrylonitrile nascent composite fibers with grafted multi walled carbon nanotubes prepared by wet spinning method. *Polymers* **2019**, *11*, 422.
(33) Helmiyati; Aprilliza, M. Characterization and properties of sodium alginate from brown algae used as an ecofriendly super-absorbent. *IOP Conf. Ser.: Mater. Sci. Eng.* **2017**, *188*, 012019.
(34) Haddad, M. Y.; Alharbi, H. F.; Karim, M. R.; Aijaz, M. O.; Alharthi, N. H. Preparation of TiO_2 incorporated polyacrylonitrile electrospun nanofibers for adsorption of heavy metal ions. *J. Polym. Res.* **2018**, *25*, 1−14.

https://doi.org/10.1021/acsabm.4c00550
ACS Appl. Bio Mater. 2024, 7, 5345−5358

(35) Deng, S.; Wang, P.; Zhang, G.; Dou, Y. Polyacrylonitrile-based fiber modified with thiosemicarbazide by microwave irradiation and its adsorption behavior for Cd (II) and Pb (II). *J. Hazard. Mater.* **2016**, *307*, 64−72.
(36) Horzum, N.; Boyací, E.; Eroglu, A. E.; Shahwan, T.; Demir, M. M. Sorption efficiency of chitosan nanofibers toward metal ions at low concentrations. *Biomacromolecules* **2010**, *11*, 3301−3308.
(37) Kim, M. S.; Kim, H. J.; Jang, J. Y.; Shin, H. S. Development of coaxial alginate-PCL nanofibrous dressing for controlled release of *Spirulina extract*. *J. Biomater. Sci. Polym. Ed.* **2018**, *29*, 1389−1400.
(38) Lee, J. S.; Jin, G. H.; Yeo, M. G.; Jang, C. H.; Lee, H.; Kim, G. H. Fabrication of electrospun biocomposites comprising polycaprolactone/fucoidan for tissue regeneration. *Carbohydr. Polym.* **2012**, *90*, 181−188.
(39) Arinstein, A.; Burman, M.; Gendelman, O.; Zussman, E. Effect of supramolecular structure on polymer nanofibre elasticity. *Nature Nanotechnol.* **2007**, *2*, 59−62.
(40) Yao, J.; Bastiaansen, C. W.; Peijs, T. High strength and high modulus electrospun nanofibers. *Fibers* **2014**, *2*, 158−187.
(41) Naraghi, M.; Arshad, S.; Chasiotis, I. Molecular orientation and mechanical property size effects in electrospun polyacrylonitrile nanofibers. *Polymer* **2011**, *52*, 1612−1618.
(42) Lagergren, S. K. About the theory of so-called adsorption of soluble substances. *Sven. Vetenskapsakad. Handingarl* **1898**, *24*, 1−39.
(43) Bulgariu, D.; Bulgariu, L. Equilibrium and kinetics studies of heavy metal ions biosorption on green algae waste biomass. *Bioresour. Technol.* **2012**, *103*, 489−493.
(44) Mahapatra, A.; Mishra, B.; Hota, G. Electrospun Fe_2O_3−Al_2O_3 nanocomposite fibers as efficient adsorbent for removal of heavy metal ions from aqueous solution. *J. Hazard. Mater.* **2013**, *258*, 116−123.
(45) Davis, T. A.; Volesky, B.; Mucci, A. A review of the biochemistry of heavy metal biosorption by brown algae. *Water Res.* **2003**, *37*, 4311−4330.
(46) Karim, M. R.; Aijaz, M. O.; Alharth, N. H.; Alharbi, H. F.; Al-Mubaddel, F. S.; Awual, M. R. Composite nanofibers membranes of poly (vinyl alcohol)/chitosan for selective lead (II) and cadmium (II) ions removal from wastewater. *Ecotoxicol. Environ. Saf.* **2019**, *169*, 479−486.
(47) Zhang, S.; Shi, Q.; Christodoulatos, C.; Meng, X. Lead and cadmium adsorption by electrospun PVA/PAA nanofibers: Batch, spectroscopic, and modeling study. *Chemosphere* **2019**, *233*, 405−413.
(48) Nordin, N. A.; Abdul Rahman, N.; Abdullah, A. H. Effective removal of Pb (II) ions by electrospun PAN/Sago lignin-based activated carbon nanofibers. *Molecules* **2020**, *25*, 3081.
(49) Canbolat, M. F.; Channa, A. M.; Baytak, S. Synthesis of Titanium Oxide Incorporated Polyvinyl Pyrrolidone Nanofibers (PVPT) and Remediation of Lead from Water System. *Fibers Polym.* **2020**, *21*, 2473−2478.
(50) Hamad, A. A.; Hassouna, M. S.; Shalaby, T. I.; Elkady, M. F.; Abd Elkawi, M. A.; Hamad, H. A. Electrospun cellulose acetate nanofiber incorporated with hydroxyapatite for removal of heavy metals. *Int. J. Biol. Macromol.* **2020**, *151*, 1299−1313.
(51) Khashij, M.; Mohammadi, P.; Babei, M.; Mehralian, M.; Aghamohammadi, N. Process optimization and modeling of lead removal using maleate/PAN nanocomposite nanofibers: characterization, kinetics and isotherm studies. *Desalination Water Treat* **2021**, *210*, 330−339.
(52) Mohammed, Y. A.; Ma, F.; Liu, L.; Zhang, C.; Dong, H.; Wang, Q.; Xu, X.; Al-Wahbi, A. A. Preparation of electrospun polyvinylidene fluoride/amidoximized polyacrylonitrile nanofibers for trace metal ions removal from contaminated water. *J. Porous Mater.* **2021**, *28*, 383−392.
(53) HMTShirazi, R.; Mohammadi, T.; Asadi, A. A. Incorporation of amine-grafted halloysite nanotube to electrospun nanofibrous membranes of chitosan/poly (vinyl alcohol) for Cd (II) and Pb (II) removal. *Appl. Clay Sci.* **2022**, *220*, 106460.
(54) Syed, N.; Feng, Y.; Mahar, F. K.; Fahad, R.; Abro, Z. A.; Huang, J. Facile synthesize of composite for pollutant removal of lead and methylene blue (MB). *Environmental Progress & Sustainable Energy* **2024**, *43*, e14317.
(55) Talukder, M. E.; Pervez, M.; Jianming, W.; Stylios, G. K.; Hassan, M. M.; Song, H.; Naddeo, V.; Figoli, A.; et al. Ag nanoparticles immobilized sulfonated polyethersulfone/polyethersulfone electrospun nanofiber membrane for the removal of heavy metals. *Sci. Rep.* **2022**, *12*, 1−16.
(56) Herath, H. K. Removal of Heavy Metals from Water Using Natural Bauxite. *Ph.D. thesis*, The University of Mississippi, 2021; p 95.
(57) Okpara, O. G.; Ogbeide, O. M.; Ike, O. C.; Menechukwu, K. C.; Ejike, E. C. Optimum isotherm by linear and nonlinear regression methods for lead (II) ions adsorption from aqueous solutions using synthesized coconut shell−activated carbon (SCSAC). *Toxin Rev.* **2021**, *40*, 901−914.
(58) Biçer, G.; Gonen, F. Telon Blue AGLF Adsorption by NiO Based Nanomaterials: Equilibrium, Kinetic And Thermodynamic Approach. *J. Turkish Chem. Soc. Sect. Chem.* **2017**, *4*, 675−690.
(59) Tonk, S.; Rápó, E. Linear and nonlinear regression analysis for the adsorption of remazol dye by Romanian brewery waste by-product, *Saccharomyces cerevisiae*. *Int. J. Mol. Sci.* **2022**, *23*, 11827.
(60) Batool, F.; Akbar, J.; Iqbal, S.; Noreen, S.; Bukhari, S. N. A. Study of isothermal, kinetic, and thermodynamic parameters for adsorption of cadmium: an overview of linear and nonlinear approach and error analysis. *Bioinorg. Chem. Appl.* **2018**, *2018*, 1−11.
(61) Başaran Kankiliç, G.; Metin, A. Ü.; Aluç, Y.; Bozkaya, O. Bioremoval of mercury (II) from aqueous solutions by *Phragmites australis*: kinetic and equilibrium studies. *J. Dispers. Sci. Technol.* **2018**, *39*, 1790−1799.
(62) Kankílíç, G. B.; Metin, A. Ü. Phragmites australis as a new cellulose source: Extraction, characterization and adsorption of methylene blue. *J. Mol. Liq.* **2020**, *312*, 113313.
(63) Marrakchi, F.; Hameed, B.; Hummadi, E. Mesoporous biohybrid epichlorohydrin crosslinked chitosan/carbon−clay adsorbent for effective cationic and anionic dyes adsorption. *Int. J. Biol. Macromol.* **2020**, *163*, 1079−1086.
(64) Sahmoune, M. N. Evaluation of thermodynamic parameters for adsorption of heavy metals by green adsorbents. *Environ. Chem. Lett.* **2019**, *17*, 697−704.
(65) Fourest, E.; Volesky, B. Contribution of sulfonate groups and alginate to heavy metal biosorption by the dry biomass of Sargassum fluitans. *Environ. Sci. Technol.* **1996**, *30*, 277−282.
(66) Liang, R.-h.; Li, Y.; Huang, L.; Wang, X.-d.; Hu, X.-x.; Liu, C.-m.; Chen, M.-s.; Chen, J. Pb^{2+} adsorption by ethylenediamine-modified pectins and their adsorption mechanisms. *Carbohydr. Polym.* **2020**, *234*, 115911.
(67) Jafarnejad, M.; Asli, M. D.; Taromi, F. A.; Manoochehri, M. Synthesis of multi-functionalized Fe_3O_4-NH_2-SH nanofiber based on chitosan for single and simultaneous adsorption of Pb (II) and Ni (II) from aqueous system. *Int. J. Biol. Macromol.* **2020**, *148*, 201−217.
(68) Li, Y.; Zhang, Z.; Liu, X.; Che, S.; Shi, N.; Chen, Y.; Yan, M. Adsorption behavior and mechanism of Lead (Pb^{2+}) by sulfate polysaccharide from Enteromorpha prolifera. *Int. J. Biol. Macromol.* **2022**, *207*, 760−770.
(69) Maccaferri, E.; Cocchi, D.; Mazzocchetti, L.; Benelli, T.; Brugo, T. M.; Giorgini, L.; Zucchelli, A. How Nanofibers Carry the Load: Toward a Universal and Reliable Approach for Tensile Testing of Polymeric Nanofibrous Membranes. *Macromol. Mater. Eng.* **2021**, *306*, 2100183.
(70) Aksil, T.; Abbas, M.; Trari, M.; Benamara, S. Water adsorption on lyophilized Arbutus unedo L. fruit powder: Determination of thermodynamic parameters. *Microchem. J.* **2019**, *145*, 35−41.

https://doi.org/10.1021/acsabm.4c00550
ACS Appl. Bio Mater. 2024, 7, 5345−5358